

Mouse model carrying H222P-*Lmna* mutation develops muscular dystrophy and dilated cardiomyopathy similar to human striated muscle laminopathies

Takuro Arimura^{1,2,†}, Anne Helbling-Leclerc^{1,2,†}, Catherine Massart^{1,2}, Shaida Varnous^{1,2}, Florence Niel^{1,2}, Emmanuelle Lacène^{1,2}, Yves Fromes^{1,2}, Marcel Toussaint³, Anne-Marie Mura⁴, Dagmar I. Keller^{1,2}, Helge Amthor⁵, Richard Isnard^{2,6}, Marie Malissen⁴, Ketty Schwartz^{1,2} and Gisèle Bonne^{1,2,*}

¹Inserm UR582, Institut de Myologie, GH Pitié-Salpêtrière, 75013 Paris, France, ²Inserm IFR14, GH Pitié-Salpêtrière, Paris, France, ³Service des Maladies Cardiovasculaires, Centre Hospitalier Général, 91160 Longjumeau, France, ⁴Centre d'Immunologie de Marseille-Luminy, Inserm-CNRS-Université de la Méditerranée, Parc Scientifique de Luminy, 13000 Marseille, France, ⁵Veterinary Basic Sciences, The Royal Veterinary College, London NW1 OTU, UK and ⁶Service de Cardiologie, GH Pitié-Salpêtrière, 75013 Paris, France

Received September 30, 2004; Revised and Accepted November 5, 2004

Laminopathies are a group of disorders caused by mutations in the *LMNA* gene encoding A-type lamins, components of the nuclear lamina. Three of these disorders affect specifically the skeletal and/or cardiac muscles, and their pathogenic mechanisms are still unknown. We chose the *LMNA* H222P missense mutation identified in a family with autosomal dominant Emery–Dreifuss muscular dystrophy, one of the striated muscle-specific laminopathies, to create a faithful mouse model of this type of laminopathy. The mutant mice exhibit overtly normal embryonic development and sexual maturity. At adulthood, male homozygous mice display reduced locomotion activity with abnormal stiff walking posture and all of them die by 9 months of age. As for cardiac phenotype, they develop chamber dilation and hypokinesia with conduction defects. These abnormal skeletal and cardiac features were also observed in the female homozygous mice but with a later-onset than in males. Histopathological analysis of the mice revealed muscle degeneration with fibrosis associated with dislocation of heterochromatin and activation of Smad signalling in heart and skeletal muscles. These results demonstrate that *Lmna*^{H222P/H222P} mice represent a good model for studying laminopathies affecting striated muscles as they develop a dystrophic condition of both skeletal and cardiac muscles similar to the human diseases.

INTRODUCTION

The nuclear lamina is a fibrous meshwork of type V intermediate filaments, the lamins, localized at the internal face of the inner nuclear membrane. This structure is fundamental in sustaining the structural integrity and mechanical stability of the nuclear envelope. Lamins are also localized within the nuclear matrix (1). In mammals, up to seven different lamins

exist: A-type lamins (A, AΔ10, C and C2 encoded by *LMNA* gene through alternative splicing) and B-type lamins (B1 and B2/B3, which are transcribed from the *LMNB1* and *LMNB2* genes, respectively). Whereas B-type lamins are present in both embryonic and differentiated cells, A-type lamins are expressed only in later stages of development and in differentiated cells. Lamins have binding affinity with chromatin and integral proteins of the inner nuclear membrane, such as

*To whom correspondence should be addressed at: Inserm UR582, Institut de Myologie, Bâtiment Babinski, Groupe Hospitalier Pitié-Salpêtrière, 47 boulevard de l'Hôpital, 75651 Paris Cedex 13, France. Tel: +33 142165723; Fax: +33 142165700; Email: g.bonne@myologie.chups.jussieu.fr

†The authors wish it to be known that, in their opinion, the first two authors should be regarded as joint First Authors.

emerin. In addition to their involvement in nuclear stability, it has been suggested that lamins play important roles in DNA replication, chromatin organization, regulation of gene expression, spatial organization of the nuclear pore and the correct anchorage of the nuclear envelope proteins (2).

We identified the first *LMNA* mutations in the autosomal dominant form of Emery–Dreifuss muscular dystrophy (AD-EDMD) highlighting the unpredicted role of these proteins in the pathophysiology of neuromuscular disorders (3). Since then, within 5 years, mutations in this gene have been identified to be responsible for up to nine disorders, i.e. dilated cardiomyopathy with conduction-system disease (DCM-CD) (4), limb girdle muscular dystrophy with atrioventricular conduction disturbance (LGMD1B) (5), Dunnigan-type of familial partial lipodystrophy (6), autosomal recessive Charcot–Marie–Tooth disease type 2 (7), mandibuloacral dysplasia (8), Hutchinson–Gilford progeria syndrome (HGPS) (9,10), atypical Werner’s syndrome (11) and restrictive dermopathy (12). This group of human hereditary diseases are now recognized as laminopathies and are characterized by the extreme variability of the phenotypes associated with the wide spectrum of *LMNA* gene mutations. Some phenotypic overlaps between the various types of laminopathies were also demonstrated (13,14). The mechanisms by which mutations in the *LMNA* gene encoding ubiquitously expressed proteins cause these various tissue-specific disorders remain to be elucidated.

Among laminopathies three disorders, EDMD, LGMD1B and DCM-CD, affect specifically the skeletal and/or cardiac muscles (3–5). The diagnosis of this type of laminopathy is particularly important because of the severity of the cardiac symptoms, characterized by conduction defect, arrhythmias, left ventricular (LV) dysfunction and dilation with heart failure. As >40% of these patients die suddenly, implantation of a cardioverter-defibrillator is necessary to prevent sudden cardiac death (15,16). The identification of the precise molecular mechanisms of *LMNA* mutations leading to laminopathies affecting striated muscles is critical for developing new therapeutic strategies to prevent cardiac dysfunction and sudden death.

At the present time, two genetically engineered mouse strains with modified *Lmna* gene have been reported. Lamin A/C null mice (*Lmna*^{-/-}) were created to analyse the functional importance of lamin A/C in the end stages of embryonic development and regulation of the terminal differentiation (17). The replacement of exon 8–11 of *Lmna* gene by *Pgkneo* cassette leads to the loss of lamin A/C expression that is not embryonic lethal but leads to the development of muscular dystrophy, DCM and death by 8 weeks of age (17,18). The other genetically engineered mice were created with the aim of producing an EDMD model with the introduction of the *LMNA* L530P mutation that causes AD-EDMD in human. Very surprisingly, *Lmna*^{L530P/L530P} mice presented clinical defects consistent with human HGPS, including a reduction in growth rate, pathologies of bone, muscle and skin and death by 4 weeks of age (19). These two genetically engineered mouse strains developed some features of the human disorders but failed to reproduce faithfully any type of human laminopathy from the gene mutation to the clinical features.

In the present paper, we chose a missense mutation (H222P) identified in a family with a typical AD-EDMD (20) to create a *Lmna* knock-in mouse, with the aim of producing a faithful

animal model of striated muscle laminopathies. We introduced the c.665A > C, p.H222P mutation in the *Lmna* murine gene by homologous recombination. Although mice carrying this point mutation do not show any phenotypes in neonatal and sexual maturity stages, at adulthood homozygous mutant (*Lmna*^{H222P/H222P}) mice develop muscular dystrophy and DCM-CD similar to the clinical features of human laminopathies affecting the striated muscles, with all *Lmna*^{H222P/H222P} mice dying by 13 months of age.

RESULTS

mRNA and protein expression of lamins A/C and emerin

Lmna^{H222P} mice were created by homologous recombination using standard techniques and the targeting constructs described in Materials and Methods section and Figure 1A. After heterozygous intercrossing, we obtained *Lmna*^{H222P/H222P}, *Lmna*^{H222P/+} and wild-type (WT) mice. We first checked the mRNA expression levels of lamins A/C and emerin in the LV and skeletal muscles (gastrocnemius and quadriceps) by quantitative RT–PCR techniques. We observed neither differences for lamin A/C and emerin mRNA expression levels nor splicing abnormality of lamin A and C mRNAs between WT, *Lmna*^{H222P/+} and *Lmna*^{H222P/H222P} mice (data not shown). We then checked the amount of lamins A/C and emerin proteins and detected similar amounts of lamins A/C and emerin in both LV and gastrocnemius muscle of *Lmna*^{H222P/+} and *Lmna*^{H222P/H222P} mice as compared to WT mice (Fig. 1D).

Lmna^{H222P/H222P} mice have a reduced life expectancy and die during adulthood, whereas *Lmna*^{H222P/+} mice have a life expectancy comparable to WT mice

Analysis of 133 newborn mice from 15 independent heterozygous crosses indicated that the numbers of mice with the three genotypes WT, H222P/+ and H222P/H222P were 39/56/38, approximating the expected ratio of 1 : 2 : 1 of Mendelian inheritance of the genotype. Both the mutated *Lmna*^{H222P/H222P} and *Lmna*^{H222P/+} mice were indistinguishable from their WT siblings at birth and seemed healthy during the sexual maturity stage, indicating that the H222P mutation is not lethal during embryonic and perinatal stages and has no impact on the general health condition at young-age.

At adulthood, *Lmna*^{H222P/H222P} male mice weighed less than WT and *Lmna*^{H222P/+} male mice and their growth rate was reduced after 3 months of age, despite normal feeding habits (Fig. 2B). At this time, *Lmna*^{H222P/H222P} male mice began to show progressively abnormal phenotypes characterized by a hunched position, stiff walking posture and rapid shallow breathing, and all *Lmna*^{H222P/H222P} male mice died between 4 and 9 months of age (Fig. 2D). As for female mice, *Lmna*^{H222P/H222P} mice were slightly lighter than WT and *Lmna*^{H222P/+} mice (Fig. 2C), and also exhibited abnormal phenotypes similar to *Lmna*^{H222P/H222P} male mice but only after 6 months of age. The first *Lmna*^{H222P/H222P} female mouse died at 7 months of age, and all *Lmna*^{H222P/H222P} female mice were dead by 13 months of age (Fig. 2D). *Lmna*^{H222P/+} mice were indistinguishable from WT mice with regard to phenotype and life expectancy.

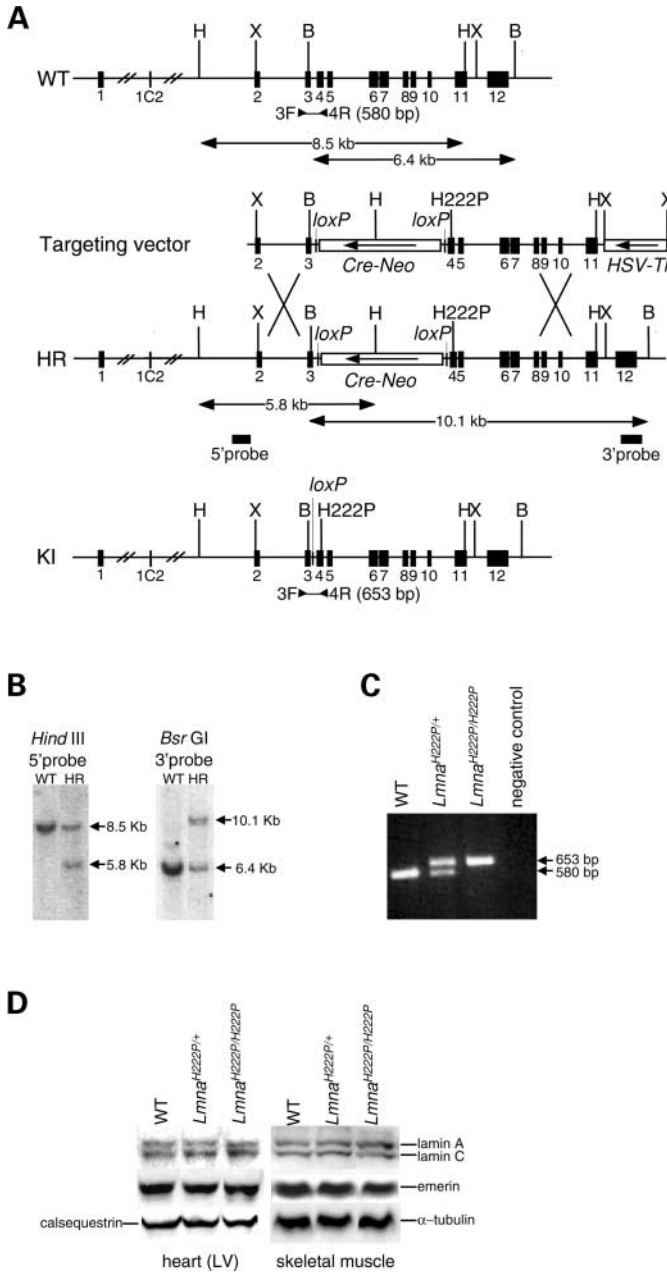


Figure 1. Gene targeting of the *Lmna* gene. (A) Schematic structure of the wild-type *Lmna* gene (WT), targeting vector, homologous recombinant containing the *Cre/Neo-loxP* cassette (HR) and targeted allele (KI). The arrows indicate the orientation of Phage P1 (*Cre*), neomycin resistance (*Neo*) and herpes simplex virus-thymidine kinase (*HSV-Tk*) genes. Positions of restriction enzyme sites and probes used for Southern blot analysis are shown. H, *Hind*III; B, *Bsr*GI; X, *Xho*I. (B) Detection of WT and HR cells by Southern blot analysis. DNAs from electroporated ES cells were digested with *Hind*III or *Bsr*GI and analysed by Southern blot analyses with 5' or 3' probes, respectively, as shown in (A). The fragments of 5.8 and 8.5 kb for 5' probe as well as 6.4 and 10.1 kb for 3' probe represent WT and HR alleles, respectively. (C) Genotyping by PCR. DNAs prepared from tail were analysed by 3F and 4R primers as shown in (A). The 580 and 653 bp bands represent WT and KI alleles, respectively. (D) Western blot detection of lamins A/C and emerin in WT, *Lmna*^{H222P/+} and *Lmna*^{H222P/H222P} mice heart (left ventricular, LV) and skeletal muscle (gastrocnemius) showing no difference in lamin A/C and emerin expression levels between different genotypes. Internal controls, caldesquestrin and β -tubulin for heart and skeletal muscle, respectively, confirmed equal loading of samples.

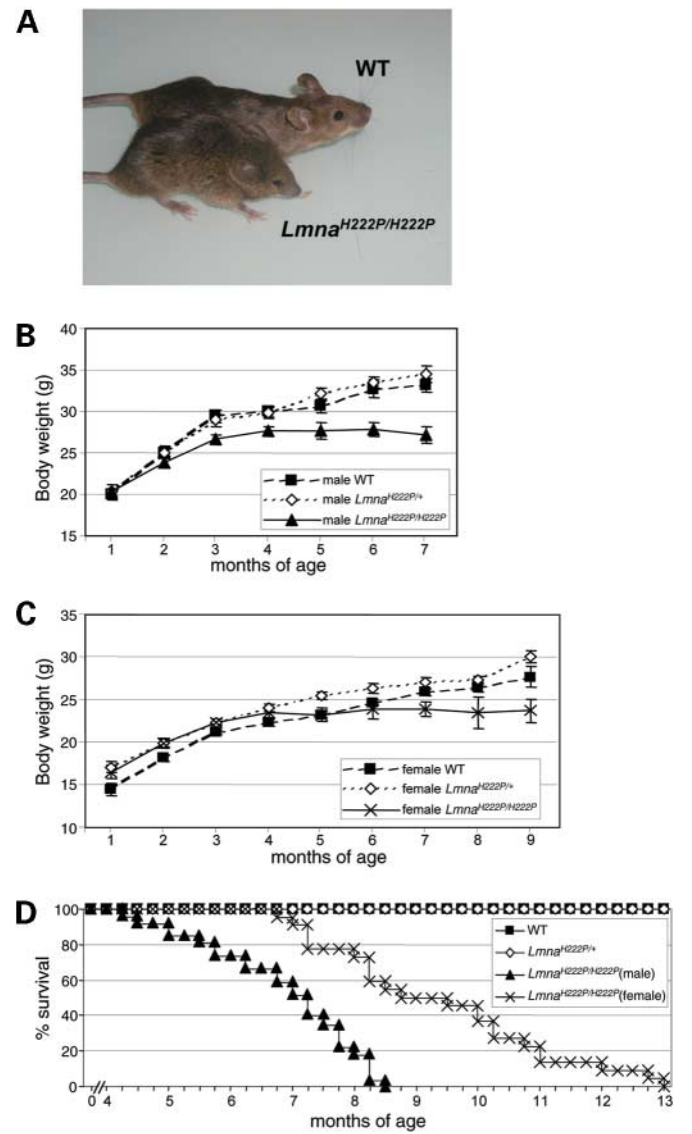


Figure 2. Overall phenotype of the *Lmna* mutant animals. (A) Picture of WT (up) and *Lmna*^{H222P/H222P} (down) males at 5 months of age. (B) Growth curves of male mice: WT (closed squares, n = 20), *Lmna*^{H222P/+} (open diamonds, n = 20) and *Lmna*^{H222P/H222P} (closed triangles, n = 9, still alive at 7 months of age). Male *Lmna*^{H222P/H222P} mice show reduction of BW gain after 3 months of age. (C) Growth curves of female mice: WT (closed squares, n = 20), *Lmna*^{H222P/+} (closed diamonds, n = 20) and *Lmna*^{H222P/H222P} (crosses, n = 9, still alive at 9 months of age). Female *Lmna*^{H222P/H222P} mice have slight reduction of BW gain. (D) Cumulative survival curve of mice: WT (closed squares, n = 40 for males and females), *Lmna*^{H222P/+} (open diamonds, n = 40 for males and females), male *Lmna*^{H222P/H222P} (closed triangles, n = 27) and female *Lmna*^{H222P/H222P} (crosses, n = 23). *Lmna*^{H222P/H222P} mice have significantly reduced life spans when compared with WT mice.

***Lmna*^{H222P/H222P} mice develop DCM with atrio-ventricular conduction abnormality**

For the assessment of cardiac abnormality, we performed echocardiography in the mice at 2, 4 and 6 (male/female) and 8 months (female) of age (Tables 1 and 2) and systolic blood pressure measurement by indirect tail-cuff sphygmomanometer

Table 1. Echocardiographic data for male WT and *Lmna*^{H222P/H222P} mice aged 2, 4 and 6 months

	2 months of age		4 months of age		6 months of age	
	WT (n = 5)	<i>Lmna</i> ^{H222P/H222P} (n = 7)	WT (n = 7)	<i>Lmna</i> ^{H222P/H222P} (n = 12)	WT (n = 7)	<i>Lmna</i> ^{H222P/H222P} (n = 8)
BW (g)	27.2 ± 1.07	23.9 ± 0.83*	30.8 ± 1.30	27.0 ± 0.82*	34.7 ± 1.43	28.3 ± 1.63*
IVSd (mm)	0.500 ± 0.010	0.514 ± 0.014	0.514 ± 0.014	0.483 ± 0.011	0.543 ± 0.030	0.500 ± 0.010
PWd (mm)	0.580 ± 0.037	0.557 ± 0.020	0.543 ± 0.020	0.500 ± 0.021	0.529 ± 0.018	0.471 ± 0.029
LVM (mg)	54.3 ± 6.14	60.8 ± 3.11	66.1 ± 4.70	71.0 ± 4.45	77.0 ± 7.24	82.5 ± 5.14
LVM/BW (mg/g)	2.02 ± 0.27	2.56 ± 0.13	2.15 ± 0.13	2.63 ± 0.15*	2.23 ± 0.21	2.69 ± 0.54
LVEDD (mm)	3.40 ± 0.17	3.69 ± 0.13	3.89 ± 0.08	4.26 ± 0.14*	4.19 ± 0.14	4.73 ± 0.17*
LVESD (mm)	1.94 ± 0.14	2.43 ± 0.17	2.43 ± 0.10	3.16 ± 0.20**	2.41 ± 0.12	4.04 ± 0.24***
LVEDD/BW (mm/g)	0.126 ± 0.009	0.155 ± 0.006*	0.127 ± 0.004	0.159 ± 0.006**	0.122 ± 0.007	0.174 ± 0.017**
LVESD/BW (mm/g)	0.072 ± 0.007	0.102 ± 0.007*	0.080 ± 0.006	0.117 ± 0.007**	0.070 ± 0.004	0.150 ± 0.018**
LVFS (%)	43.1 ± 2.2	34.6 ± 2.7*	37.4 ± 2.7	26.5 ± 2.5**	42.4 ± 1.9	15.1 ± 2.2***
Heart rate (bpm)	520 ± 14	490 ± 14	468 ± 31	526 ± 19	549 ± 22	556 ± 22

Cardiac function was evaluated by transthoracic echocardiographic analyses of the left ventricle: LVM/BW, LV mass-to-body weight ratio; LVEDD/BW, LV end-diastolic diameter-to-body weight ratio; LVESD/BW, LV end-systolic diameter-to-body weight ratio; LVFS, LV fractional shortening.

**P* < 0.05 versus WT.

***P* < 0.01 versus WT.

****P* < 0.001 versus WT.

method in male mice at 2 months of age. Although systolic blood pressure was not modified in *Lmna*^{H222P/H222P} male mice (120.9 ± 1.4 versus 127.5 ± 8.6 mmHg in WT mice; *n* = 5 for each groups, *P* = 0.45), *Lmna*^{H222P/H222P} male mice developed a progressive LV dilation associated with a progressive decrease of contractile function, evidenced by decreased LV fractional shortening (LVFS), which was significant at 2 months of age (Fig. 3B and Table 1). The development of LV dysfunction was not accompanied with cardiac LV hypertrophy (Table 1). Similar features were observed in female *Lmna*^{H222P/H222P} mice but with a later-onset (Table 2). Indeed, the LV dysfunction in female homozygous mutant mice appeared at 4 months of age and seemed to progress less rapidly than in males (Tables 1 and 2). Both male and female *Lmna*^{H222P/+} mice had no cardiac dysfunction by 1 year of age (data not shown).

Telemetric ambulatory electrocardiogram (ECG) measurements were performed in homozygous mutant and WT male mice at 3, 4 and 5 months of age (Table 3). Abnormalities of the conduction system were observed: *Lmna*^{H222P/H222P} male mice at 3 months of age showed a significant increase of the PR interval when compared with WT male mice, indicating atrio-ventricular conduction defects. This increase of PR interval remained stable at 4 and 5 months of age. The QRS complex duration, as a parameter for intraventricular conduction, was significantly increased between *Lmna*^{H222P/H222P} and WT male mice at 5 months of age. In addition, frequent sinoatrial blocks and ventricular extra-systoles were observed in male *Lmna*^{H222P/H222P} mice at 5 months of age during recording. Such abnormalities were never observed in the age-matched WT mice (data not shown).

Gross examination and histopathological analysis of the hearts were performed at the end stage of the disease on several *Lmna*^{H222P/H222P} mice at 4, 5, 6 and 7 months of age for males and at 7 and 10 months of age for females. In each case, the same abnormalities were observed in these mice and typical abnormalities are presented in Figure 3. Macroscopically, the mice had dramatically enlarged hearts with dilation of the atria (Fig. 3D). Microscopically, ventricular chamber

dilation was obvious (Fig. 3F). Histopathologically, a prominent alteration observed in the heart of *Lmna*^{H222P/H222P} mice was a marked increase of fibrosis. In addition, single or small clusters of cardiac muscle cells with degeneration and necrosis were extensively present in the left and right ventricles in *Lmna*^{H222P/H222P} mice (Fig. 3H). There was no evidence of cellular hypertrophy, disarray or inflammatory cells.

Histopathological analysis of the heart of 1 year *Lmna*^{H222P/+} mice revealed no abnormalities (data not shown).

Lmna^{H222P/H222P} mice have abnormal locomotion activities

The influence of the H222P mutation also became apparent in the locomotion activity of the mice, as evidenced in the open field test and rotarod assay. The spontaneous locomotion activity at 6 months of age, tested in open field, was significantly impaired in male *Lmna*^{H222P/H222P} mice compared to WT but was normal in females (Fig. 4A). The *Lmna*^{H222P/H222P} female mice exhibited reduced spontaneous locomotion activity at 8 months of age, moving only 6.4 ± 2.0% of the time when compared with 54.8 ± 3.4% of the time spent in motion for WT female mice (*P* < 0.001, *n* = 3). In a rotarod assay at 6 months of age, both male and female *Lmna*^{H222P/H222P} mice fell earlier from the rotarod, whereas WT mice managed to stay on the rotarod up to 2 min (Fig. 4B). Similar results were also observed for females at 8 months of age (4.4 ± 1.3% in *Lmna*^{H222P/H222P} versus 100% in WT, *P* < 0.001, *n* = 5). The *Lmna*^{H222P/+} mice had normal locomotion activities compared to WT by 1 year of age (data not shown).

Lmna^{H222P/H222P} mice exhibit dystrophic pattern of skeletal muscles

Histological and histochemical analyses were performed on skeletal muscles at the end stage of the disease on several *Lmna*^{H222P/H222P} mice at 4, 5, 6 and 7 months of age for males and at 7 and 10 months of age for females. We analyzed

Table 2. Echocardiographic data for female WT and *Lmna*^{H222P/H222P} mice aged 2, 4, 6 and 8 months

	2 months of age		4 months of age		6 months of age		8 months of age	
	WT (n = 5)	<i>Lmna</i> ^{H222P/H222P} (n = 4)	WT (n = 12)	<i>Lmna</i> ^{H222P/H222P} (n = 12)	WT (n = 11)	<i>Lmna</i> ^{H222P/H222P} (n = 12)	WT (n = 11)	<i>Lmna</i> ^{H222P/H222P} (n = 9)
BW (g)	20.4 ± 0.68	22.0 ± 0.82	21.4 ± 0.65	23.9 ± 0.58	22.5 ± 0.55	24.8 ± 0.58	24.7 ± 1.21	25.7 ± 0.55
IVSd (mm)	0.500 ± 0.032	0.525 ± 0.025	0.496 ± 0.010	0.492 ± 0.008	0.500 ± 0.013	0.492 ± 0.015	0.482 ± 0.012	0.456 ± 0.018
PWd (mm)	0.520 ± 0.020	0.475 ± 0.025	0.492 ± 0.015	0.467 ± 0.019	0.545 ± 0.016	0.500 ± 0.010*	0.545 ± 0.016	0.489 ± 0.020*
LVM (mg)	46.3 ± 3.53	53.3 ± 1.42	48.7 ± 1.81	61.8 ± 2.86**	57.8 ± 1.74	62.3 ± 2.87	53.7 ± 2.30	68.2 ± 6.2*
LVM/BW (mg/g)	2.27 ± 0.14	2.43 ± 0.05	2.28 ± 0.08	2.60 ± 0.12	2.58 ± 0.06	2.52 ± 0.10	2.19 ± 0.09	2.68 ± 0.27
LVEDD (mm)	3.26 ± 0.16	3.60 ± 0.14	3.44 ± 0.08	4.03 ± 0.12***	3.64 ± 0.08	3.94 ± 0.11*	3.53 ± 0.06	4.26 ± 0.18**
LVESD (mm)	1.72 ± 0.07	2.18 ± 0.18	2.17 ± 0.09	2.84 ± 0.12***	2.15 ± 0.05	2.93 ± 0.17***	2.07 ± 0.06	3.40 ± 0.26***
LVEDD/BW (mm/g)	0.160 ± 0.004	0.164 ± 0.004	0.162 ± 0.005	0.169 ± 0.005	0.164 ± 0.004	0.160 ± 0.005	0.146 ± 0.006	0.167 ± 0.009
LVESD/BW (mm/g)	0.084 ± 0.003	0.099 ± 0.006	0.101 ± 0.003	0.120 ± 0.007*	0.097 ± 0.003	0.118 ± 0.006*	0.085 ± 0.004	0.134 ± 0.012**
LVFS (%)	46.9 ± 2.6	39.9 ± 2.6	37.2 ± 1.6	29.3 ± 2.3*	40.9 ± 1.2	26.3 ± 2.4***	41.2 ± 1.6	21.0 ± 2.7***
Heart rate (bpm)	574 ± 21	541 ± 24	511 ± 27	509 ± 19	526 ± 11	479 ± 24	527 ± 6	523 ± 17

Cardiac function was evaluated by transthoracic echocardiographic analyses of the left ventricle: LVM/BW, LV mass-to-body weight ratio; LVEDD/BW, LV end-diastolic diameter-to-body weight ratio; LVESD/BW, LV end-systolic diameter-to-body weight ratio; LVFS, LV fractional shortening.

* $P < 0.05$ versus WT.

** $P < 0.01$ versus WT.

*** $P < 0.001$ versus WT.

muscles of fore and hind legs to search for proximal and/or distal defects as in AD-EDMD patients (20) and diaphragm muscle as the mice exhibited rapid shallow breathing. Severe cytoarchitectural abnormalities of muscle associated with an increase of connective tissue were observed in the diaphragm and soleus muscles of the *Lmna*^{H222P/H222P} mice (Fig. 5B, D and F). Moderate abnormalities were also observed in other skeletal muscles including gastrocnemius, quadriceps, triceps and tibialis anterior (data not shown). These abnormalities were observed in both male and female *Lmna*^{H222P/H222P} mice. Compared to WT, muscle tissue carrying the homozygous mutation exhibited a wide variation in fibre size with an increased number of atrophic fibres, hypertrophic fibres and lobulated fibres as well as some regenerative muscle fibres. Some fibres also showed increased numbers of nuclei with internal localization. Reaction for myofibrillar ATPase localization demonstrated that atrophic/degenerated fibres were of both type 1 and type 2 fibres and exhibited loss of ATPase staining (Fig. 5H). We also observed that almost all the hypertrophic muscle fibres were type 2. Mitochondrial cytochrome *c* oxidase and succinate dehydrogenase staining demonstrated focal loss of enzyme activity prominently in atrophic/degenerated fibres (Fig. 5J and L). Haematoxylin and eosin (H&E) staining of skeletal muscles of *Lmna*^{H222P/+} mice revealed a normal histological pattern compared to WT by 1 year of age (data not shown).

Lmna^{H222P/H222P} mice do not exhibit biochemical features of lipodystrophy

To evaluate metabolic characteristics of the *Lmna*^{H222P/H222P} mice, serum glucose, total cholesterol, high density lipoprotein cholesterol, low density lipoprotein, triglycerides, uric acids, aspartate aminotransferase and alanine aminotransferase were measured at 6–8 months of age. In male *Lmna*^{H222P/H222P} mice, glucose and insulin levels tended to be lower when compared with male WT mice, although a significant difference was observed only for glucose (Table 4). In female *Lmna*^{H222P/H222P} mice, only triglycerides levels were significantly higher than in female WT mice. Decreased glucose levels in males (and to a lesser extent in females) and increased triglyceride levels in females might be a consequence of muscle loss and/or impaired growth, although it is rather difficult to evaluate to what extent this may contribute to the global phenotype. We did not observe any significant differences of low density lipoprotein, uric acids, aspartate aminotransferase and alanine aminotransferase in both male and female *Lmna*^{H222P/H222P} mice compared to sex-matched WT (data not shown). Thus, neither male nor female *Lmna*^{H222P/H222P} mice developed biochemical features of lipodystrophy at adulthood.

Lmna^{H222P/H222P} mice do not exhibit any lipid metabolism abnormalities in affected tissues

In *Lmna*^{H222P/H222P} mice, the prominent alteration in affected muscles is an increase of fibrosis with degeneration and necrosis of muscle cells. Because abnormalities of lipid metabolism lead to lipoapoptosis of myocytes and development of cardiomyopathy (21), and a few EDMD patients presented some

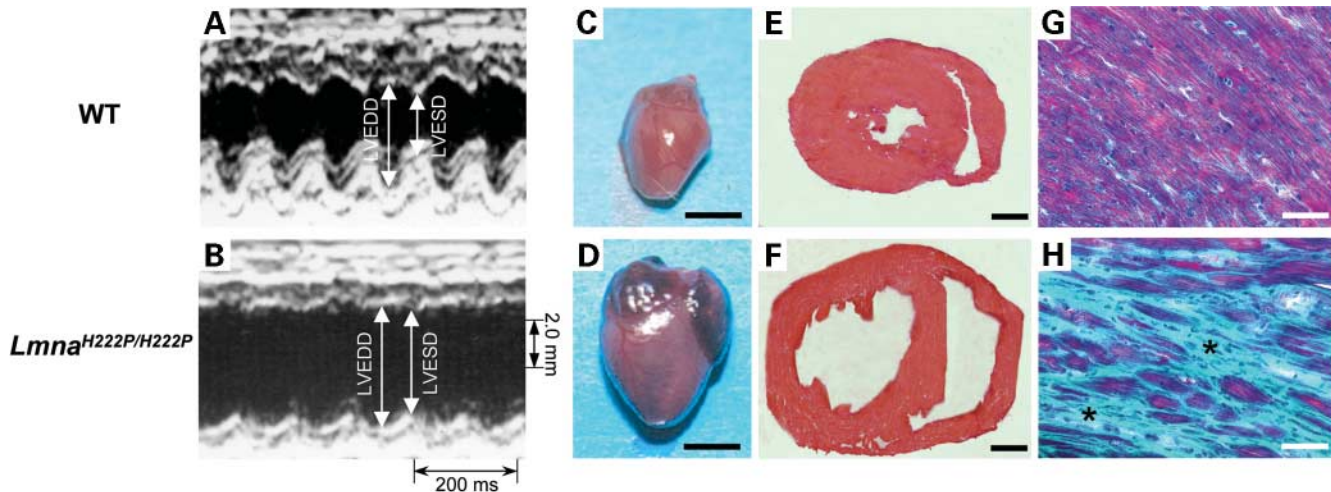


Figure 3. Cardiac phenotype in the male *Lmna*^{H222P/H222P} mice at 6 months of age. (A and B) Transthoracic M-mode echocardiographic tracings in a male WT (A) and male *Lmna*^{H222P/H222P} (B) mouse. Double-sided vertical arrows indicate the end-diastolic diameter of LV chamber (LVEDD). The smaller adjacent arrows indicate the end-systolic diameter of LV chamber (LVESD). Note LV dilation and reduced systolic contraction in *Lmna*^{H222P/H222P} mouse. (C and D) Hearts from WT (C) and *Lmna*^{H222P/H222P} (D) male mice. Dilatation of both atria and ventricles is present in the *Lmna*^{H222P/H222P} mouse (D); scale bar = 5 mm. (E and F) Transversal sections through the hearts of the mice show both left and right ventricular dilation in *Lmna*^{H222P/H222P} mouse (F) compared to WT (E) (H&E stain); scale bar = 1 mm. (G and H) Histopathological analysis of *Lmna*^{H222P/H222P} mouse heart (H) with modified Gomori's trichrome stain reveal extensive degeneration of myocytes and massive fibrosis (green, asterisk) compared to WT (G); scale bar = 50 μ m.

Table 3. ECG data for WT and *Lmna*^{H222P/H222P} male mice aged 3, 4 and 5 months

	3 months of age		4 months of age		5 months of age	
	WT (n = 3)	<i>Lmna</i> ^{H222P/H222P} (n = 3)	WT (n = 3)	<i>Lmna</i> ^{H222P/H222P} (n = 4)	WT (n = 5)	<i>Lmna</i> ^{H222P/H222P} (n = 3)
PR interval (ms)	35.3 \pm 0.94	42.4 \pm 2.22*	36.2 \pm 1.13	41.1 \pm 0.96*	36.5 \pm 0.72	41.1 \pm 1.92*
QRS duration (ms)	11.9 \pm 0.72	12.1 \pm 0.1	11.8 \pm 0.32	12.8 \pm 0.94	11.1 \pm 0.34	18.7 \pm 0.35***

**P* < 0.05 versus WT.

****P* < 0.001 versus WT.

features of lipodystrophy (13), we hypothesized that fatty acid accumulation may contribute to the development of these phenotypes in *Lmna*^{H222P/H222P} mice. Oil Red O staining to determine lipid accumulation was performed at the early stage of the disease on several *Lmna*^{H222P/H222P} mice, i.e. at 2 and 3 months of age for males and females and at the end stage of the disease, i.e. at 4, 5, 6 and 7 months of age for males and at 7 and 10 months of age for females. However, no lipid accumulation was observed in any *Lmna*^{H222P/H222P} mice (data not shown). Also, there was no difference in LV and skeletal muscle SREBP1 and PPAR γ mRNA levels between WT, *Lmna*^{H222P/+} and *Lmna*^{H222P/H222P} male mice. Thus, *Lmna*^{H222P/H222P} mice did not develop any abnormal features of lipid metabolism in affected tissues.

Normal localizations of lamins A/C and emerin proteins is observed in the *Lmna*^{H222P/H222P} mice

Localization of lamin A/C and emerin proteins in striated muscle sections was evaluated at 6 months of age. Immunohistochemical analyses of lamins A/C and emerin localizations in the heart (Fig. 6D–F) and gastrocnemius muscle (Fig. 6J–L)

of *Lmna*^{H222P/H222P} mice showed similar localization of these proteins compared to heart and muscle of WT mice (Fig. 6A–C and G–I, respectively). Normal localization of these proteins was also observed in other skeletal muscles (diaphragm, soleus, quadriceps, triceps) (data not shown).

Lmna^{H222P/H222P} mice exhibit alteration of heterochromatin distribution in cardiac and skeletal muscles

We analyzed the ultrastructure in cardiac and quadriceps muscles by electron microscopy. The general architecture of the myocytes was normal, the myofibrils were not disrupted and the distribution of mitochondria was normal. Approximately 10% of the nuclei showed pathologic changes in both heart and quadriceps (Fig. 7A and B). The heterochromatin appeared to be very dark, highly condensed and with an irregular distribution. We did not observe caryoplasm extrusion. Sometimes the nuclear membrane showed deep convolutions, with the appearance of intranuclear tubules. These abnormalities were also observed in satellite cells, fibroblasts and endothelial cells of capillaries (Fig. 7C and D).

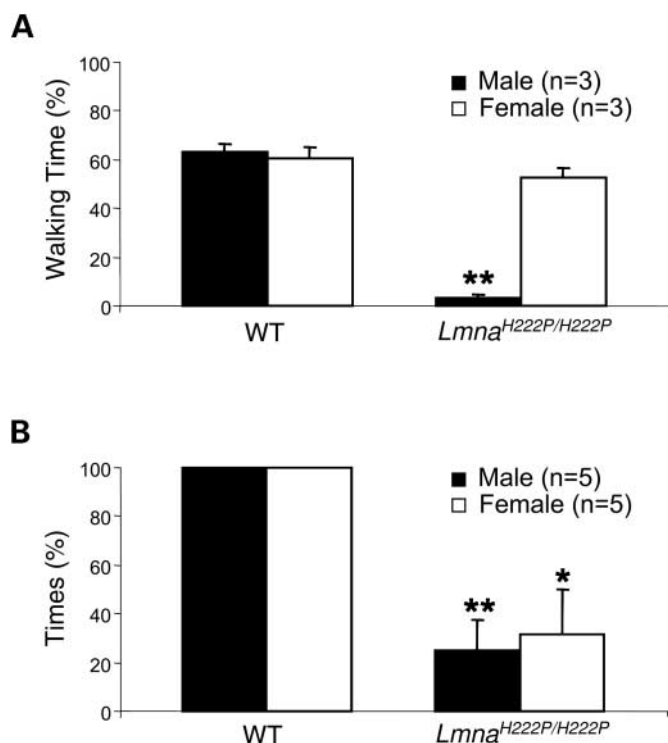


Figure 4. Locomotion activities of the mice at 6 months of age. (A) Exploratory locomotion activity of WT and *Lmna*^{H222P/H222P} mice in open field test for 5 min ($n = 3$ for each group). (B) Rotarod assays performed in WT and *Lmna*^{H222P/H222P} mice for 2 min ($n = 5$ for each group). Black bars and white bars represent the results in males and females, respectively. * $P < 0.01$ versus sex-matched WT; ** $P < 0.001$ versus sex-matched WT.

Lmna^{H222P/H222P} mice exhibit increased nuclear translocation of Smad proteins in cardiac and skeletal muscles

A significant body of literature indicates that TGF- β_1 is a powerful initiator for fibrosis, extracellular matrix deposition and alteration of gene expression in heart (22). The intracellular effectors of TGF- β signalling, the Smad proteins, when activated via TGF- β receptors, translocate into the nucleus where they regulate gene transcription. Briefly, receptor-activated Smad proteins, such as Smad2 and Smad3, are phosphorylated and form a heteromeric complex with Smad4. These phosphorylated Smad2/3–Smad4 dimers then translocate to the nucleus, mediating the target gene responses (22). Previous studies demonstrated elevated levels of Smad proteins and increased nuclear accumulation of phosphorylated Smad2 (P-Smad2) in failing heart, strongly suggesting that activation of the Smad proteins is associated with fibrosis in failing heart (23,24).

We hypothesized that pathologic alterations of the nuclear envelope promoted by the *Lmna* mutation in *Lmna*^{H222P/H222P} mice might alter the intranuclear import of Smad proteins and hence might contribute to the striated muscle phenotype, especially the extensive fibrosis observed in both skeletal and cardiac muscles. Immunofluorescence staining of heart and diaphragm muscles from 5, 6 and 7 months of age males and 10 months of age female mice revealed that

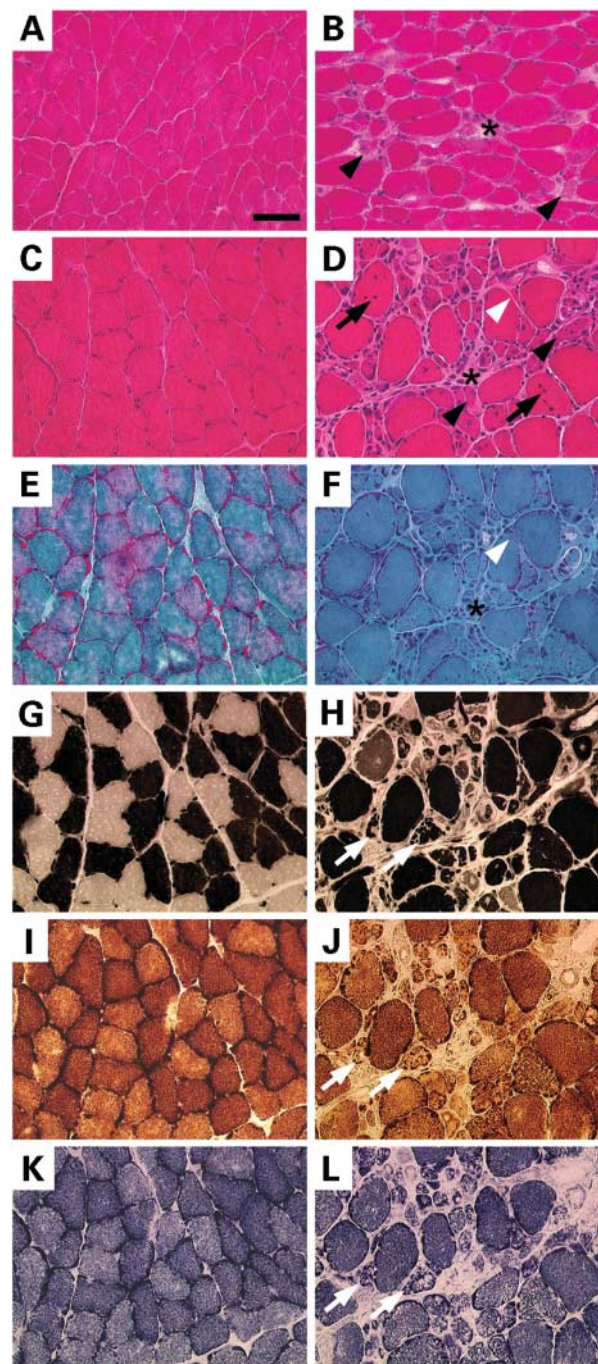


Figure 5. Histological and histochemical analysis of skeletal muscles from male WT (A, C, E, G, I and K) and *Lmna*^{H222P/H222P} (B, D, F, H, J and L) mice at 6 months of age. Fresh frozen diaphragm (A and B) and soleus muscles (C–L) from WT and *Lmna*^{H222P/H222P} mice were stained with H&E (A–D), modified Gomori trichrome (E and F) or myofibrillar ATPase, pH 9.3 (G and H), cytochrome *c* oxidase (I and J) and succinate dehydrogenase (K and L) activity. (A–F) Variability in fibre size with hypertrophic muscle cells and numerous degenerative fibres (black arrowheads) were observed in both diaphragm (b) and soleus (d) muscles in *Lmna*^{H222P/H222P} mice when compared with WT. In addition, the presence of interstitial fibrosis (asterisk), splitting muscle fibres (white arrowheads) and internal nuclei (black arrows) are indicated. (G–L) White arrows in *Lmna*^{H222P/H222P} muscle indicate abnormal reaction for myofibrillar ATPase at pH 9.4 (H). This abnormality is associated with focal loss of mitochondrial cytochrome *c* oxidase activity (J) and succinate dehydrogenase activity (L); scale bar = 50 μ m.

Table 4. Blood chemistry data of WT and *Lmna*^{H222P/H222P} mice aged 6–8 months

Sex	Genotype	n	Glucose (mmol/l)	TC (mmol/l)	HDL-C (mmol/l)	Triglycerides (mmol/l)	Insulin (μ g/l)
M	WT	6	3.92 \pm 0.36	3.03 \pm 0.32	2.19 \pm 0.27	0.62 \pm 0.05	1.04 \pm 0.3
M	<i>Lmna</i> ^{H222P/H222P}	6	2.00 \pm 0.31**	3.20 \pm 0.36	2.10 \pm 0.18	0.98 \pm 0.18	0.50 \pm 0.1
F	WT	6	3.02 \pm 0.50	3.41 \pm 0.30	2.40 \pm 0.22	0.77 \pm 0.06	0.48 \pm 0.13
F	<i>Lmna</i> ^{H222P/H222P}	6	2.16 \pm 0.43	2.61 \pm 0.24	1.79 \pm 0.21	1.34 \pm 0.16**	0.71 \pm 0.13

Blood biochemistry was measured after 6 months of age. The mice were matched for body weight; TC, total cholesterol; HDL-C, high density lipoprotein cholesterol.

***P* < 0.01 versus sex-matched WT.

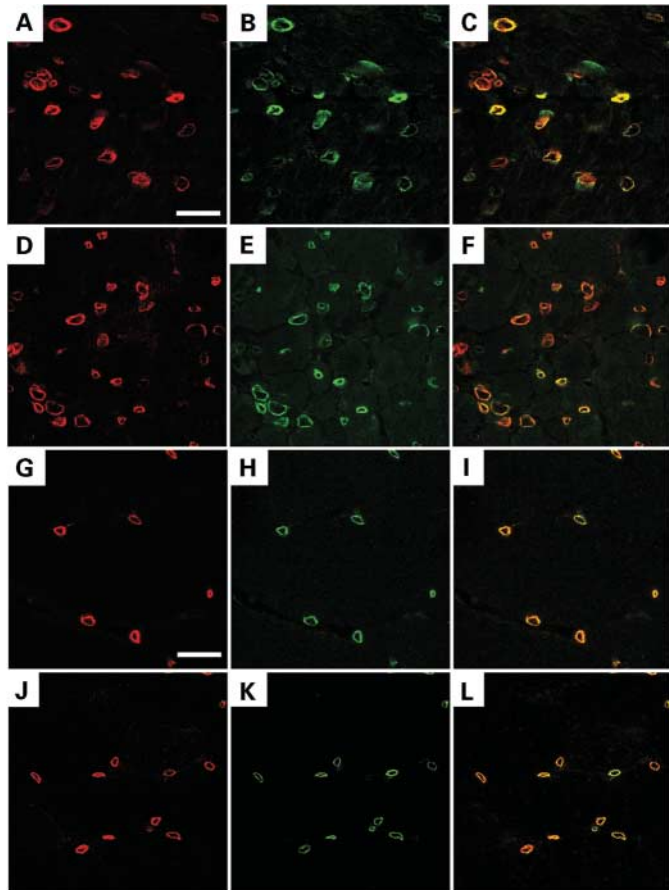


Figure 6. Immunodetection of lamins A/C and emerin in heart and skeletal muscles from male mice at 6 months of age. Immunostaining with lamin A/C Ab (A, D, G and J), emerin Ab (B, E, H and K) and overlay (C, F, I and L) show the localization of nuclear envelope proteins in heart and gastrocnemius muscle of WT (A, B, C, G, H and I) and *Lmna*^{H222P/H222P} mice (D, E, F, J, K and L). In WT mice, lamin A/C (A and G) and emerin (B and H) proteins were co-localized at nuclear periphery in heart (C) and gastrocnemius muscle (I). In heart and gastrocnemius muscle of *Lmna*^{H222P/H222P} mice, similar lamin A/C (D and J) and emerin (E and K) co-localization (F and L) compared to WT were observed, respectively; scale bar = 20 μ m.

phosphorylated Smad2/3 proteins (P-Smad2/3) were equally distributed in both cytoplasm and nucleus in heart and skeletal muscle of WT (Fig. 8A–D and I–L, respectively) and *Lmna*^{H222P/+} mice (data not shown). In contrast, P-Smad2/3 detection in *Lmna*^{H222P/H222P} mouse tissues revealed an accumulation of P-Smad2/3 in nuclei, with brightly stained

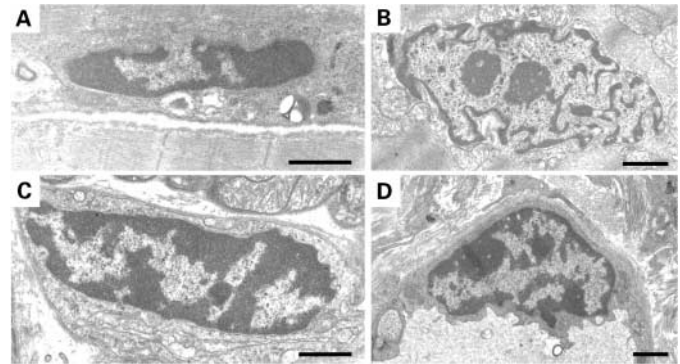


Figure 7. Nuclear morphology analysis of heart and quadriceps muscle from male *Lmna*^{H222P/H222P} mice at 6 months of age. (A) Central deposit of densely stained heterochromatin in the myocyte of quadriceps muscle. (B) Deep indentations of the nuclear membrane in cardiomyocyte. (C and D) Condensation of heterochromatin close to the membrane in fibroblast of the heart (C) and in endothelial cell of a capillary (D) of the heart; scale bar = 1 μ m.

regions co-localizing with nuclei of both myofibres and fibrosis areas (Fig. 8E–H and M–P, respectively). These staining patterns of P-Smad2/3 were not observed on phosphatase-treated tissue sections (data not shown). This increase of translocation of Smad proteins in the nuclei was confirmed by western blot analysis. The protein amounts of total Smad2 (phosphorylated and non-phosphorylated) and Smad4 from LV tissues of female mice of 9–12 months of age were determined after cell fractionation. In *Lmna*^{H222P/H222P} LV tissues, the amounts of Smad2 and Smad4 proteins were increased in the nuclear fraction when compared with WT and *Lmna*^{H222P/+} mouse hearts (Fig. 9).

DISCUSSION

In the present study, we developed *Lmna* knock-in mice carrying the H222P mutation that was identified in the human *LMNA* gene in a family with typical AD-EDMD (20). We show that at adulthood homozygous mutant mice, *Lmna*^{H222P/H222P}, develop muscular dystrophy and DCM associated with conduction defects, reminiscent of EDMD in human. Cardiac and skeletal muscle dysfunctions have a later-onset in female than in male *Lmna*^{H222P/H222P} mice. This is the first *Lmna* mouse model mimicking human laminopathy from the gene mutation to the clinical features.

As we wanted to reproduce human pathologic conditions, we precisely reproduced a human *LMNA* gene mutation in the

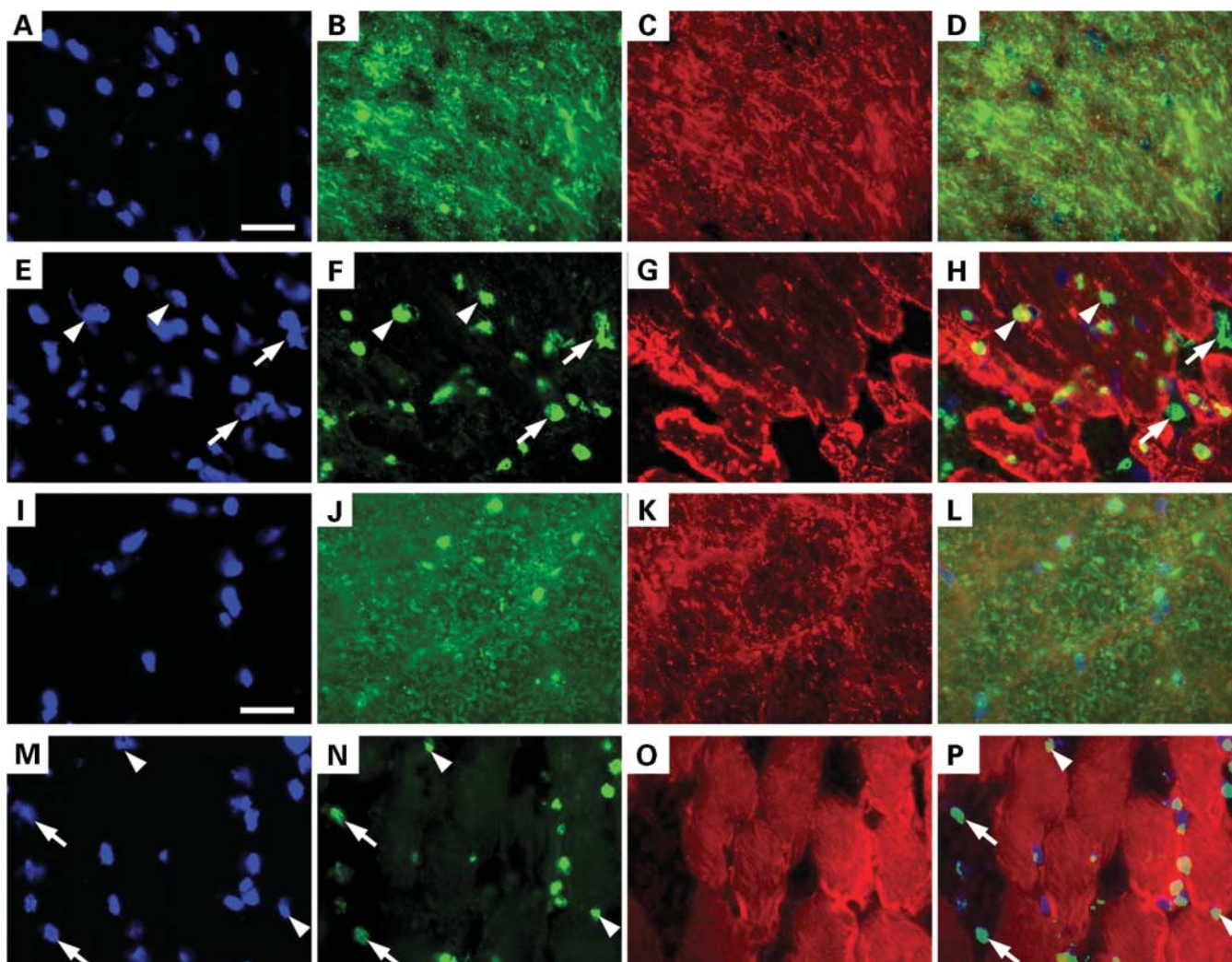


Figure 8. Immunohistochemical analysis of P-Smad2/3 in heart and skeletal muscles from male mice at 6 months of age. Immunohistostainings with P-Smad2/3 Ab (B, F, J and N), desmin Ab (C, G, K and O) and overlay (D, H, L and P) show the localization of P-Smad2/3 proteins in heart (A–H) and diaphragm (I–P) of WT (A–D and I–L) and *Lmna*^{H222P/H222P} (E–H and M–P) mice. Nuclei in each tissue section were stained with DAPI (A, E, I and M). In WT mice, P-Smad2/3 proteins were localized at both cytosol and nuclei in heart (B) and diaphragm (J). In *Lmna*^{H222P/H222P} mice, P-Smad2/3 proteins showed predominant intranuclear distribution in heart and diaphragm (F and N, respectively). This staining pattern was observed in both myocytes (white arrowheads in desmin positive area) and non-myocyte cells (white arrows in desmin negative area); scale bar = 20 μ m. Identical results were obtained in heart and diaphragm tissue sections from male mice at 5 and 7 months of age and female mice at 10 months of age (data not shown).

mouse genome: the same single nucleotide base change (CAT>CCT) in exon 4 of the murine *Lmna* gene and of the human *LMNA* gene directs the same amino acid replacement from histidine to proline at codon 222 in the murine lamins A/C as in the human proteins (c.665A>C, p.H222P) (20).

The previous mouse model developed with the same aim, i.e. *Lmna*^{L530P} knock-in mice as an AD-EDMD mouse model, led surprisingly to the development of clinical features highly reminiscent of another type of human laminopathy, the HGPS (19). HGPS is a premature ageing syndrome with a median age at death of 13.4 years, clinically characterized by postnatal growth retardation, midface hypoplasia, micrognathia, cardiovascular disease, absence of subcutaneous fat, alopecia and generalized osteodysplasia (9,10). The majority of HGPS cases are caused by the single *LMNA* point mutation

G608G leading to the aberrant activation of a cryptic donor splice site in exon 11 (9,10,25). Unexpectedly, the introduction of the AD-EDMD L530P mutation in the mouse genome produced a reduction in growth rate and pathologies of bone, muscle and skin, and *Lmna*^{L530P/L530P} mice died by 4 weeks of age (19). Actually, similar to human HGPS, these progeria-like features were associated with greatly diminished levels of mutant lamin A/C mRNA and proteins due to aberrant splicing (19). The phenotype differences observed between *Lmna*^{H222P/H222P} and *Lmna*^{L530P/L530P} mice are most probably due to the difference in the expression of mutated protein. Indeed, *Lmna*^{H222P/H222P} mice demonstrated a normal expression level of both mutated lamin A/C mRNA and proteins. The observation for the first time of normal expression level of mutated lamin A/C in a *Lmna*

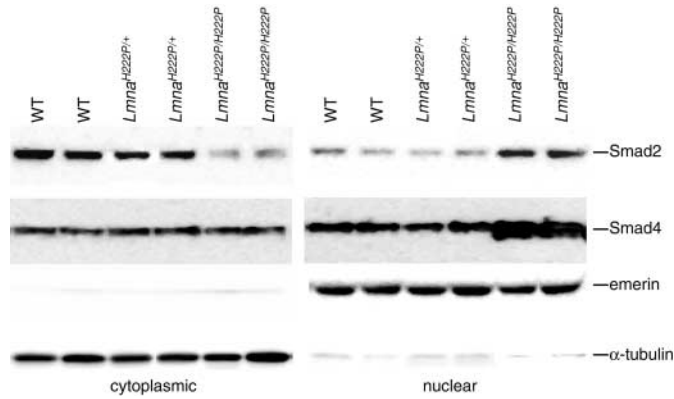


Figure 9. Smad proteins localization in LV of female mice at 9–12 months of age. Representative data for two WT, *Lmna*^{H222P/+} and *Lmna*^{H222P/H222P} mice are shown. Experiments were repeated at least three times with three mice from each group. Cytoplasmic and nuclear fractions of LV tissue were solved on SDS–PAGE and hybridized with Ab against total Smad2 (phosphorylated + non-phosphorylated forms) and Smad4 proteins. When compared with WT and *Lmna*^{H222P/+} mice, *Lmna*^{H222P/H222P} mice show increased amounts of Smad2 and Smad4 proteins in the nuclear fractions and decreased amount of total Smad2 proteins in the cytoplasmic fraction. Detection of α -tubulin (cytoplasmic protein) and emerlin (nuclear protein) confirms that the cytoplasmic and nuclear fractions were correctly separated.

mouse model carrying an AD-EDMD mutation suggests that stability of the mutated lamins A/C may be important for developing a laminopathy specifically affecting striated muscles in mice.

The other genetically engineered mice, i.e. *Lmna* null mice (*Lmna*^{-/-}), although not reproducing a human *LMNA* mutation, develop some features of human laminopathies (7,17,18,26). Regarding striated muscle laminopathy, *Lmna*^{-/-} mice present rapid onset of muscular dystrophy associated with progressive DCM and death by 8 weeks of age (17,18). There are several points of similarity between *Lmna*^{-/-} and *Lmna*^{H222P/H222P} mice such as abnormal growth curve, abnormal gait, muscle weakness, dystrophic muscles, DCM-CD and abnormal chromatin organization. However, there are also critical differences between the two strains as detailed in Table 5. The main difference is the later-onset and the less rapid progression of both muscular dystrophy and DCM-CD in *Lmna*^{H222P/H222P}, mimicking the human pathology more closely. Thus, the progression of the disease can be studied in more detail, particularly in the heart. Indeed, PR interval is increased in *Lmna*^{H222P/H222P} male mice in the early stage of DCM at 3 months of age, indicating atrio-ventricular conduction defects, whereas QRS duration increases at 5 months of age, indicating intraventricular conduction disturbance, probably due to the marked increase of fibrosis and cardiac chamber dilation at this stage of the disease. In contrast, the *Lmna*^{-/-} mice had normal cardiac ECG and echocardiography parameters at 2 weeks, exhibited DCM with prolongations of both PR interval and QRS duration at 4–6 weeks of age and died at 8 weeks (18). Thus, the disease of the *Lmna*^{H222P/H222P} mice quite closely mimics human cardiac disease, in which atrio-ventricular conduction defects are most frequently the first cardiac symptoms in patients, DCM arising usually later during progression of the cardiac

Table 5. Comparison of striated muscles phenotype in *Lmna*^{H222P/H222P}, *Lmna*^{-/-} mice and human

	<i>Lmna</i> ^{H222P/H222P} mice	<i>Lmna</i> ^{-/-} mice ^a	Striated muscle laminopathy in human
Gene defect	Missense <i>Lmna</i> mutation	Deletion of <i>Lmna</i> exon 8–11	80% of missense <i>LMNA</i> mutation (15)
Disease expression mode	Only homozygous mice are affected	Only homozygous mice are affected	Majority of AD forms, very rare autosomal recessive forms (43)
mRNA expression level	Normal	Highly decreased	??
Lamin A/C expression and localization	Normal	Absent	Normal for missense mutation (56), haploinsufficiency for nonsense mutation (27)
Ultrastructure analysis	Normal	Present but with abnormal localization	Normal in muscle biopsies (3,56,57)
Contractures and abnormal gait	Abnormal heterochromatin organization	Changes in nuclear morphology and heterochromatin organization	Chromatin reorganization in skeletal muscle (56,58), nucleoplasm extrusion in cardiomyocyte (29)
Locomotion activity	Abnormal gait with a stiff walking posture	Abnormal gait with a stiff walking posture	Abnormal gait with early contractures in EDMD and late minimal contractures in LGMD1B (30)
Muscular weakness and dystrophic features	Greatly impaired	??	Patients could lose ambulation in severe cases (15)
Progressive dilated cardiomyopathy	Diaphragm, soleus, gastrocnemius, quadriceps, triceps and tibialis anterior	Perivertebral, rectus femoris and semimembranosus muscles	Humero-peroneal muscles weakness in EDMD; limb-girdle muscles weakness in LGMD1B (30), dystrophic features in muscle biopsies from deltoid or quadriceps (30,59)
Conduction defects	At 2 months in males, at 4 months in females	At 1 month	After 2nd decade (15)
Myocard histology	At 3 months in male	At 1 month	After 2nd decade (15)
Death	Degenerated myocytes, important fibrosis	No necrosis, no fibrosis	Myocyte damage, interstitial fibrosis (29)
Feature of partial lipodystrophy	At 4–9 months for male, at 7–13 months for female	At 2 months	High frequency of cardiac death after 2nd decade (16)
Gender difference	No insulin resistance	No insulin resistance	Some patients may exhibit some features of partial lipodystrophy (13)
	Yes	No	Not reported

^aFrom Sullivan *et al.* (17), Nikolova *et al.* (18) and Cutler *et al.* (26).

disease (16,27–31). These cardiac dysfunctions are associated with cardiomyocyte degeneration and a marked increase of interstitial fibrosis in the *Lmna*^{H222P/H222P} mouse hearts. These features were not observed in *Lmna*^{-/-} mouse hearts (18) but were reported in patients in whom cardiac histopathological analysis was performed (4,29,32). Significant dystrophic features and fibrosis were also present in the diaphragm of *Lmna*^{H222P/H222P} mice associated with rapid shallow breathing; this muscle being largely unaffected in the *Lmna*^{-/-} mice (18). Histological analysis of diaphragm in patients has never been reported. Diaphragm biopsies are not performed in patients, and respiratory investigations are not routinely carried out most probably due to the fact that respiratory insufficiency is not a hallmark of striated muscle laminopathy. In order to evaluate further such impairment in patients, we retrospectively analyzed clinical details of patients who had systematic respiratory investigations. Among 57 cases, seven were identified with severe impairment of respiratory function (33,34). This result suggests that involvement of the diaphragm or accessory respiratory muscles may be underestimated in human striated muscle laminopathy, further investigations are needed to confirm these first results.

A striking feature is the death between 4 and 13 months of age of the *Lmna*^{H222P/H222P} mice. Death was most probably due to a combination of arrhythmia, end-stage heart failure due to DCM with decreased LVFS and respiratory failure as a consequence of weak performance of dystrophic diaphragm. All the *Lmna*^{-/-} mice died even earlier at 2 months of age (17) probably due to the more rapidly progressive cardiac disease, although arrhythmia and diaphragm defects were not reported in the *Lmna*^{-/-} mice (17,18).

Interestingly, the weaker performance of heart and skeletal muscles and early death in *Lmna*^{H222P/H222P} mice had a later-onset in females than in males *Lmna*^{H222P/H222P} mice. This gender difference was not reported in *Lmna*^{-/-} mice, although the early death by 2 months of age may prevent the detection of discrepancies between males and females. Several gene-targeted mouse strains demonstrated that male mice displayed more pronounced abnormalities in cardiac function than females (35–39). It was suggested that steroid-hormones, such as testosterone and estrogens, may explain these gender differences in cardiac dysfunction (40,41). On the other hand, gender differences in mouse strains with skeletal muscle disorders seem to be unknown. We provide here the first evidence of sex-related survival benefits in an animal model of cardiac and skeletal myopathy. Although the mechanism by which this may occur is still unknown, one could hypothesize that ovarian hormones may play a protective role in the onset of disease in females or testicular hormones may accelerate the development of phenotypes in males in this mouse model. Future studies using ovariectomy or castration of the *Lmna*^{H222P/H222P} mice may further elucidate these mechanisms. Additional studies are also needed to determine whether such gender difference may exist in human affected by striated muscle laminopathies, as it has not been reported yet for EDMD, LGMD1B or DCM-CD.

Surprisingly, *Lmna*^{H222P/+} mice showed no abnormalities up to 1 year of age despite the fact that the majority of patients reported so far with striated muscle-specific laminopathy carry

heterozygous *LMNA* mutation. There are numerous precedents for mouse models of human disease for which the mice presenting clinical phenotypes carry homozygous mutated alleles, whereas the patients are heterozygous for the mutated allele (42), just as we observed in the present study, with only *Lmna*^{H222P/H222P} mice developing a dystrophic condition in skeletal muscles and heart. Similarly the other two genetically engineered mice for the *Lmna* gene, *Lmna*^{-/-} and *Lmna*^{L530P} knock-in mice, exhibit clinical features only when they carry homozygous *Lmna* mutations (17,19). This may reflect different downstream pathways of the gene mutation between human and mouse. However, homozygous H222Y *LMNA* mutation in human leads to AR-EDMD (43). Although the substituted amino acids are different (proline or tyrosine), the modification of arginine 222 in lamins A/C seems to be particularly sensitive to the development of diseases in both human and mouse. Also, we cannot completely exclude the possibility that *Lmna*^{H222P/+} mice may develop abnormal phenotypes with advanced age. Further studies will be required to characterize any clinical features of human laminopathies in *Lmna*^{H222P/+} mice.

All differences observed between *Lmna*^{-/-} and *Lmna*^{H222P/H222P} mice are probably due to the distinction between complete loss of lamins A/C function (*Lmna*^{-/-}) and alteration of the function by the existence of particular mutant alleles (*Lmna*^{H222P/H222P}). Development of other knock-in *Lmna* mouse models with introduction of an EDMD mutation localized in the N-terminal domain of lamins A/C is in progress. Further comparison between phenotypes of each gene-engineered mouse model and human striated muscle-specific laminopathies may throw light on the pathogenesis of this type of laminopathy.

One of the specific and important features of *Lmna*^{H222P/H222P} mice is the extensive fibrosis observed in both cardiac and skeletal muscles, a feature that was also present in patients with striated muscle laminopathies. Interestingly, the observation of abnormal intranuclear accumulation of P-Smad2/3 proteins in myocyte and non-myocyte cells in cardiac and skeletal muscles of *Lmna*^{H222P/H222P} mice may partly explain this extensive fibrosis. Indeed, similar to what has been observed in hearts of other animal models of heart failure, activation of Smad proteins in cardiac fibroblasts and myofibroblasts was reported to play important roles in cardiac fibrosis (22–24). This intranuclear accumulation of Smad proteins most probably occurs secondary to an increase of circulating TGF- β generated by the failing heart and dystrophic muscles, even if we cannot completely exclude the hypothesis of abnormal nuclear shuttling of Smad proteins through nuclear pore complexes due to mutated lamins A/C. Thus, the puzzle of pathophysiological mechanisms is far from solved. The precise downstream effects of Smad protein activation in striated muscles of *Lmna*^{H222P/H222P} mice need to be explored further. Global gene expression profiling such as gene chip analysis would be a useful tool for investigating the consequence of P-Smad2/3 and Smad4 import into myocyte nuclei.

Thus, the two main pathophysiological hypotheses proposed for laminopathies, i.e. mechanical stress and gene expression alteration (2,44) are both most probably involved in

Lmna^{H222P/H222P} mice, as was recently suggested in analyses of *Lmna*^{-/-} mice in which impaired nuclear mechanics in absence of lamins A/C lead to alterations in gene expression (18,45). But this may be accomplished through a different intracellular pathway. Further investigations are needed to elucidate the pathogenic mechanisms of the *Lmna* H222P mutation.

In summary, the homozygous knock-in mice carrying the *Lmna* H222P mutation that we have generated faithfully reproduce the most frequent types of human laminopathies, those affecting striated muscles: a missense mutation identified in human, development of the dystrophic condition in both skeletal and cardiac muscles at adulthood, normal expression and localization of lamins A/C and emerin and abnormal heterochromatin organization. An intriguing difference between men and mice is that the clinical phenotype develops in heterozygous and homozygous, respectively. In addition, although we have not solved all the molecular basis underlying the pathology, demonstration of abnormal behaviour of intracellular TGF- β effectors, the Smad proteins, within the affected tissues, i.e. the striated muscles, shed further light on the pathomechanisms of striated muscle laminopathies.

These knock-in *LMNA*^{H222P} mice represent an important animal model for studies of the pathogenesis of laminopathies specifically affecting striated muscles and provide important tools for the development of new treatment strategies, in particular for DCM.

MATERIALS AND METHODS

Production of targeted *Lmna* H222P mice

Lmna H222P KI mice were generated by homologous recombination in CK35 ES cells (46). *Lmna* genomic clones were isolated from a 129/svJ mouse BAC genomic library (Genomesystem[®]) that contains genomic fragments encompassing the whole murine *Lmna* gene. The targeting vector for the H222P missense mutation was constructed using a 6 kb *Xho*I fragment encompassing exons 2–11 of the *Lmna* gene (Fig. 1A). A *Bsr*GI–*Cl*AI PCR fragment containing the H222P mutation in exon 4 (CAT > CCT) and a new *Sall*I restriction site in intron 3 was subcloned in this 6 kb *Xho*I fragment. A *Cre/Neo-loxP* auto-deleting selection cassette was introduced in intron 3 via the new *Sall*I site (47). Addition of a thymidine kinase selection cassette after exon 11 allowed negative selection (Fig. 1A). G418^R–GANC^R resistant ES clones were selected and screened for homologous recombination by Southern blotting as indicated in Figure 1B. For the H222P mutant allele, the *Cre/Neo-loxP* cassette introduced a new *Hind*III site, resulting in *Hind*III restriction fragments of 5.8 kb, whereas the WT allele produced a 8.5 kb fragment (Fig. 1A and B). In addition to new fragments by *Hind*III restriction, longer *Bsr*GI fragments (10.1 kb) when compared with WT (6.4 kb) were also produced in the mutant allele. Recombinant ES cells were injected in Balb/c blastocysts and implanted into pseudopregnant females. Founders were bred to WT C57BL/6 females to check for germline transmission. Germline transmission of H222P mutation and self-excision of the *Cre/Neo* cassette in the germ line of chimeric mice were confirmed by PCR analyses on genomic DNA

from heterozygous animals (data not shown) (47). Subsequent breeding produced animals containing the H222P mutation but lacking the *Cre/Neo* cassette and the genotypes were detected by PCR analyses and sequencing on tail genomic DNA with the following oligonucleotides: 3F, 5'-cagccatcacctctctcttg-3' and 4R, 5'-agcaccagggagaggacagga-3' (Fig. 1C). The single *loxP* site remaining in the *Lmna* H222P allele after deletion of the *Cre/Neo* resulted in an amplified PCR product 73 bp longer than the 580 bp fragment amplified from the WT *Lmna* allele. These mice and their litter matched WT were used in all subsequent studies. All experiments were performed in accordance with the guide for the care and use of laboratory animals published by the NIH (publication No. 85-23, revised 1985).

mRNA and protein expression

After macroscopic examination of the tissues, mouse heart and skeletal muscles were dissected and rapidly frozen in liquid-nitrogen. Total RNA was extracted from LV or skeletal muscles using RNA plus reagent (Qbiogene, Illkirch, France) as described by the manufacturer. RNA concentrations and purity were determined spectrophotometrically and RNA quality further assessed by electrophoretic separation in agarose gels. mRNA expression levels for *Lmna* and *Emd* encoding emerin protein were measured by quantitative RT–PCR using the LightCycler Real Time PCR System with the LightCycler FastStart DNA Master SYBR Green I kit (Roche Diagnostic GmbH, Mannheim, Germany). mRNA expression levels for *SREBP1* and *PPARG* encoding SREBP1 and PPAR γ proteins were also determined. Expression level of mouse β -actin was used as an internal control.

For western blot analyses, frozen tissues were homogenized in a total protein extraction buffer (2% SDS, 250 mM sucrose, 75 mM urea, 1 mM dithiothreitol and 50 mM Tris–HCl, pH 7.5) with protease inhibitor (25 μ g/ml aprotinin and 10 μ g/ml leupeptin) by FastPrep System (Qbiogene). After determination of protein concentration using the BC assay kit (Uptima, Montlucon, France), total protein was separated on SDS–PAGE gels and hybridized with primary rabbit anti-lamins A/C polyclonal antibody (Ab) (1:200, Santa Cruz Biotechnology Inc., CA, USA), primary rabbit anti-emerin polyclonal Ab (1:400, kindly provided by G.E. Morris, NEWI, UK), primary rabbit anti-calnexin polyclonal Ab (1:2500, Affinity BioReagent[™], CO, USA) or primary mouse anti- α -tubulin monoclonal Ab (Sigma-Aldrich Chemie GmbH, Steinheim, Germany) and with secondary rabbit anti-mouse (for monoclonal Ab) or goat anti-rabbit (for polyclonal Ab) IgG HRP-conjugated Ab (1:2000, Dako A/S, Grostrup, Denmark). Nuclear and cytoplasmic protein fractions were extracted from frozen LV tissues using NE-PER kits (Pierce Biotechnology Inc., IL, USA). After determination of protein concentration using the BC assay kit (Uptima), proteins were separated on SDS–PAGE gels and hybridized with primary rabbit anti-Smad2 polyclonal Ab (1:100, Zymed Laboratories Inc., CA, USA), primary rabbit anti-Smad4 polyclonal Ab (1:100, Santa Cruz Biotechnology Inc.), primary rabbit anti-emerin polyclonal Ab or primary mouse anti- α -tubulin monoclonal Ab and with secondary rabbit anti-mouse or goat

anti-rabbit IgG HRP-conjugated Ab. Recognized proteins were visualized by enhanced chemiluminescence (Pierce).

Echocardiography

Transthoracic echocardiography was performed in the mice using an Acuson 128XP/10 cardiac ultrasound machine with Acuson 10 MHz linear probe (Mountain View, CA, USA) at room temperature. Mice were slightly anesthetized with 0.5–1% isoflurane (Abbott Inc., Rungis, France) in O₂. LV parameters were obtained from M-mode recordings in a modified short axis view. Interventricular septal wall thickness in diastole (IVSd), posterior wall thickness in diastole (PWd), LV end-diastolic (LVEDD) and LV end-systolic (LVESD) diameters were calculated from the mean of at least three separate cardiac cycles. On the basis of the results of each diameters, the LV mass (LVM) and the percentage of LVFS were calculated as follows: $[(IVSd + PWd + EDD)^3 - EDD^3] \times 1.055$ (48) and $(LVEDD - LVESD)/LVEDD \times 100$ (49), respectively.

Blood pressure measurement

Systolic blood pressure measurements were performed by the indirect tail-cuff sphygmomanometer method. Non-anesthetized mice, kept at 30°C, were trained for restrainers and tail-cuff inflation. Systolic blood pressure was recorded by using a PowerLab/S system connected to CHART software (A.D. Instruments, Milford, MA, USA) (50).

Electrocardiogram

Long-term telemetric ambulatory ECG were recorded in mice with implantable transmitters (ETA-F20, Data Sciences International, MN, USA). Transmitters were inserted subcutaneously in the abdominal region under anesthesia with ketamine [75 mg per kg body weight (BW) intraperitoneally], xylazine (15 mg per kg BW intraperitoneally) and midazolam (0.75 mg per kg BW intraperitoneally). The mice were placed in cages on top of a receiver for transmission of ECG signals connected to a computer for display and analysis by Dataquest™ A.R.T™ software (Data Sciences International). Telemetric ECG tracings were obtained in conscious mice during quiet awake time at daytime and the PR interval and QRS duration were measured.

Locomotion tests

We examined exploratory locomotion of mice in an open field test. In each experiment, a mouse was placed on a new wide area and the time the mouse spent moving around over 5 min was measured. For the rotating rod task, mice were tested with 16 r.p.m. to test forced locomotion activity. Each mouse was tested three times for 2 min with 30 min recovery between each test (51).

Histopathological and histochemical analyses

Fresh specimens from individual skeletal and cardiac muscles were snap frozen in liquid-nitrogen-cooled isopentane (VWR

International, Fontenay-sous-Bois, France), and stored at –80°C until further processing. Frozen sections (8 μm) of transversal cardiac and skeletal muscles were stained with H&E, modified Gomori trichrome and Oil Red O stains, and labelled for localization of myofibrillar ATPase, cytochrome *c* oxidase and succinate dehydrogenase activity by standard methods (52). Sections were analyzed by light microscopy. For immunohistochemical analysis, tissue sections were fixed for 10 min in 100% ethanol and incubated for 1 h with blocking solution (10% goat serum, 0.03% Triton-X in PBS) at room temperature. For detection of lamins A/C and emerin, primary rabbit anti-emerin polyclonal Ab (1:200, kindly provided by G.E. Morris) were diluted in an incubation buffer (1% goat serum, 0.03% Triton-X in PBS) and sections were incubated overnight at room temperature. Sections were washed three times with 0.03% Triton-X in PBS and incubated with a secondary sheep anti-rabbit IgG FITC-conjugated Ab (1:500, Amrad Biotech, Victoria, Australia) for 1 h at room temperature. After washing with 0.03% Triton-X in PBS, immunoreaction against lamin A/C proteins was then performed on the sections using Vector® M.O.M.™ Immunodetection Kit (Vector Laboratories Inc., CA, USA) according to the manufacturer's instruction. The primary and secondary antibodies used were mouse anti-lamins A/C monoclonal Ab 4A7 (1:200, kindly provided by G.E. Morris) and Alexa fluor 568 goat anti-mouse IgG₁ (1:500, Molecular Probes, Leiden, The Netherlands), respectively. For immunohistochemical analysis of P-Smad2/3 and desmin, the primary antibodies used were goat anti-P-Smad2/3 polyclonal Ab (1:100, Santa Cruz Biotechnology Inc.) and mouse anti-desmin monoclonal Ab (1:200, Dako A/S) and the secondary antibodies used were rabbit anti-goat IgG FITC-conjugated Ab (1:500, Dako A/S) and Alexa fluor 568 goat anti-mouse IgG₁, respectively. Dephosphorylation of cryostat tissue sections with alkaline phosphatase (10 U per ml at 37°C for 1 h, Promega Biosciences Inc., CA, USA) was performed to obtain a negative control of P-Smad2/3 labelling. All tissue sections were counter-stained with 4',6-diamidino-2-phenylindole dihydrochloride (DAPI), and images were collected and analyzed with confocal Leica TCS4D DMRB microscope or Carl Zeiss Axiophot2 microscope and appropriate software.

Electron microscopy

The muscle specimens (LV and quadriceps) were immediately fixed for 2 h in 2.5% cold glutaraldehyde with 0.1 M cacodylate buffer, pH 7.3. After washing in cacodylate buffer, the specimens were post-fixed in 1% osmium tetroxyde in the same buffer, dehydrated with graded series of ethanol and embedded in Epon. Then 0.7 μm thick sections were stained with toluidine blue alkaline. The ultrathin sections were stained with uranyl acetate, citrated and observed with a Philips CM 120 electron microscope at 80 kV (53).

Serum biochemical analyses

Blood samples were obtained after 18 h fasting from male and female WT and *Lmna*^{H222P/H222P} mice between 6 and 8 months of age. The following biochemical parameters were measured as previously described (54,55): glucose, total

cholesterol, high density lipoprotein cholesterol, low density lipoprotein, triglycerides, uric acids, aspartate aminotransferase and alanine aminotransferase. All tests were performed at the Institut Clinique de la Souris (Strasbourg, France).

Statistical analysis

All data were acquired and analyzed by observers who were blinded to the animals' genotypes. Continuous variables were analyzed using ANOVA and Student's *t*-test for paired values. Statistical comparisons for cardiac dimension data were made before and after normalization for BW differences. The measured values were expressed as mean \pm SEM. *P*-values of less than 0.05 were considered to be statistically significant.

ACKNOWLEDGEMENTS

We thank M.-F. Champy (Institut Clinique de la Souris, Strasbourg, France) for helpful discussion and the Institut Clinique de la Souris for technical assistance in the measurement of blood chemical analysis. We are grateful to G.E. Morris for providing antibodies. We thank A. Rouche, P. Bozin, C. Fayet, J.-P. Leroy and S. Bauche for technical assistance. We also greatly appreciate Drs M. Bloch-Faure, N.B. Romero and R. Ben Yaou for helpful discussion. This work was supported by Inserm and grants from European Union Fifth Framework (MYO-CLUSTER/EUROMEN contract no. QL61-1999-00870), 'Association Française contre les Myopathies' (AFM, grant no. 9278) and Human Frontiers Science Program (grant no. RGP0057/2001-M101). T.A. was supported by the Human Frontier Science Program grant. D.I. was supported by grants from the Swiss National Foundation and the ADUMED Foundation, Switzerland.

REFERENCES

- Foisner, R. (2003) Cell cycle dynamics of the nuclear envelope. *Sci. World J.*, **3**, 1–20.
- Hutchison, C.J. (2002) Lamins: building blocks or regulators of gene expression? *Nat. Rev. Mol. Cell. Biol.*, **3**, 848–858.
- Bonne, G., Di Barletta, M.R., Varnous, S., Becane, H., Hammouda, E.H., Merlini, L., Muntoni, F., Greenberg, C.R., Gary, F., Urtizberea, J.A. *et al.* (1999) Mutations in the gene encoding lamin A/C cause autosomal dominant Emery–Dreifuss muscular dystrophy. *Nat. Genet.*, **21**, 285–288.
- Fatkin, D., MacRae, C., Sasaki, T., Wolff, M.R., Porcu, M., Frenneaux, M., Atherton, J., Vidaillet, H.J., Spudich, S., De Girolami, U. *et al.* (1999) Missense mutations in the rod domain of the lamin A/C gene as causes of dilated cardiomyopathy and conduction-system disease. *N. Engl. J. Med.*, **341**, 1715–1724.
- Muchir, A., Bonne, G., van der Kooij, A.J., van Meegen, M., Baas, F., Bolhuis, P.A., de Visser, M. and Schwartz, K. (2000) Identification of mutations in the gene encoding lamins A/C in autosomal dominant limb girdle muscular dystrophy with atrioventricular conduction disturbances (LGMD1B). *Hum. Mol. Genet.*, **9**, 1453–1459.
- Shackleton, S., Lloyd, D.J., Jackson, S.N., Evans, R., Niermeijer, M.F., Singh, B.M., Schmidt, H., Brabant, G., Kumar, S., Durrington, P.N. *et al.* (2000) LMNA, encoding lamin A/C, is mutated in partial lipodystrophy. *Nat. Genet.*, **24**, 153–156.
- De Sandre-Giovannoli, A., Chaouch, M., Kozlov, S., Vallat, J.M., Tazir, M., Kassouri, N., Szepietowski, P., Hammadouche, T., Vandenberghe, A., Stewart, C.L. *et al.* (2002) Homozygous defects in LMNA, encoding lamin A/C nuclear-envelope proteins, cause autosomal recessive axonal neuropathy in human (Charcot–Marie–Tooth disorder type 2) and mouse. *Am. J. Hum. Genet.*, **70**, 726–736.
- Novelli, G., Muchir, A., Sangiulio, F., Helbling-Leclerc, A., Rosaria d'Apice, M., Massart, C., Capon, F., Sbraccia, P., Federici, M., Lauro, R. *et al.* (2002) Mandibuloacral dysplasia is caused by a mutation in LMNA encoding lamins A/C. *Am. J. Hum. Genet.*, **71**, 426–431.
- De Sandre-Giovannoli, A., Bernard, R., Cau, P., Navarro, C., Amiel, J., Boccacio, I., Lyonnet, S., Stewart, C.L., Munnich, A., Le Merrer, M. *et al.* (2003) Lamin A truncation in Hutchinson–Gilford progeria. *Science*, **300**, 2055.
- Eriksson, M., Brown, W.T., Gordon, L.B., Glynn, M.W., Singer, J., Scott, L., Erdos, M.R., Robbins, C.M., Moses, T.Y., Berglund, P. *et al.* (2003) Recurrent *de novo* point mutations in lamin A cause Hutchinson–Gilford progeria syndrome. *Nature*, **25**, 25.
- Chen, L., Lee, L., Kudlow, B., Dos Santos, H., Sletvold, O., Shafeghati, Y., Botha, E., Garg, A., Hanson, N., Martin, G. *et al.* (2003) LMNA mutations in atypical Werner's syndrome. *Lancet*, **362**, 440–445.
- Navarro, C., De Sandre-Giovannoli, A., Bernard, R., Boccaccio, I., Boyer, A., Genevieve, D., Hadj-Rabia, S., Gaudy-Marqueste, C., Smith, H.S., Vabres, P. *et al.* (2004) Lamin A and ZMPSTE24 (FACE-1) defects cause nuclear disorganisation and identify restrictive dermopathy as a lethal neonatal laminopathy. *Hum. Mol. Genet.*, **13**, 2493–2503.
- van der Kooij, A.J., Bonne, G., Eymard, B., Duboc, D., Talim, B., Van der Valk, M., Reiss, P., Richard, P., Demay, L., Merlini, L. *et al.* (2002) Lamin A/C mutations with lipodystrophy, cardiac abnormalities, and muscular dystrophy. *Neurology*, **59**, 620–623.
- Goizet, C., Ben Yaou, R., Demay, L., Richard, P., Bouillot, S., Rouanet, M., Hermosilla, E., Le Masson, G., Lagueny, A., Bonne, G. *et al.* (2004) A new mutation of the lamin A/C gene leading to autosomal dominant axonal neuropathy, muscular dystrophy, cardiac disease, and leucocytosis. *J. Med. Genet.*, **41**, E29.
- Bonne, G., Ben Yaou, R., Beroud, C., Boriani, G., Brown, C.A., De Visser, M., Duboc, D., Ellis, J.A., Hausmanowa-Petrusewicz, I., Lattanzi, G. *et al.* (2003) 108th ENMC International Workshop. 3rd Workshop of the MYO-CLUSTER project: EUROMEN, 7th International Emery–Dreifuss Muscular Dystrophy (EDMD) Workshop. 13–15 September 2002, Naarden, The Netherlands. *Neuromusc. Disord.*, **13**, 508–515.
- Taylor, M.R., Fain, P.R., Sinagra, G., Robinson, M.L., Robertson, A.D., Carniel, E., Di Lenarda, A., Bohlmeier, T.J., Ferguson, D.A., Brodsky, G.L. *et al.* (2003) Natural history of dilated cardiomyopathy due to lamin A/C gene mutations. *J. Am. Coll. Cardiol.*, **41**, 771–780.
- Sullivan, T., Escalante-Alcalde, D., Bhatt, H., Anver, M., Bhat, N., Nagashima, K., Stewart, C.L. and Burke, B. (1999) Loss of A-type lamin expression compromises nuclear envelope integrity leading to muscular dystrophy. *J. Cell Biol.*, **147**, 913–920.
- Nikolova, V., Leimena, C., McMahon, A.C., Tan, J.C., Chandar, S., Jogia, D., Kesteven, S.H., Michalick, J., Otway, R., Verheyen, F. *et al.* (2004) Defects in nuclear structure and function promote dilated cardiomyopathy in lamin A/C-deficient mice. *J. Clin. Invest.*, **113**, 357–369.
- Mounkes, L.C., Kozlov, S., Hernandez, L., Sullivan, T. and Stewart, C.L. (2003) A progeroid syndrome in mice is caused by defects in A-type lamins. *Nature*, **423**, 298–301.
- Bonne, G., Mercuri, E., Muchir, A., Urtizberea, A., Becane, H.M., Reca, D., Merlini, L., Wehnert, M., Boor, R., Reuner, U. *et al.* (2000) Clinical and molecular genetic spectrum of autosomal dominant Emery–Dreifuss muscular dystrophy due to mutations of the lamin A/C gene. *Ann. Neurol.*, **48**, 170–180.
- Listenberger, L.L. and Schaffer, J.E. (2002) Mechanisms of lipopoptosis: implications for human heart disease. *Trends Cardiovasc. Med.*, **12**, 134–138.
- Rosenkranz, S. (2004) TGF-beta(1) and angiotensin networking in cardiac remodeling. *Cardiovasc. Res.*, **63**, 423–432.
- Hao, J., Ju, H., Zhao, S., Junaid, A., Scammell-La Fleur, T. and Dixon, I.M. (1999) Elevation of expression of Smads 2, 3, and 4, decorin and TGF-beta in the chronic phase of myocardial infarct scar healing. *J. Mol. Cell. Cardiol.*, **31**, 667–678.
- Hao, J., Wang, B., Jones, S.C., Jassal, D.S. and Dixon, I.M. (2000) Interaction between angiotensin II and Smad proteins in fibroblasts in failing heart and *in vitro*. *Am. J. Physiol. Heart Circ. Physiol.*, **279**, H3020–H3030.

25. D'Apice, M.R., Tenconi, R., Mammi, I., van den Ende, J. and Novelli, G. (2004) Paternal origin of LMNA mutations in Hutchinson–Gilford progeria. *Clin. Genet.*, **65**, 52–54.
26. Cutler, D.A., Sullivan, T., Marcus-Samuels, B., Stewart, C.L. and Reitman, M.L. (2002) Characterization of adiposity and metabolism in Lmna-deficient mice. *Biochem. Biophys. Res. Commun.*, **291**, 522–527.
27. Bécane, H.-M., Bonne, G., Varnous, S., Muchir, A., Ortega, V., Hammouda, E.H., Urtizberea, J.-A., Lavergne, T., Fardeau, M., Eymard, B. *et al.* (2000) High incidence of sudden death with conduction system and myocardial disease due to lamins A and C gene mutation. *Pacing Clin. Electrophysiol.*, **23**, 1661–1666.
28. Vytopil, M., Benedetti, S., Ricci, E., Galluzzi, G., Dello Russo, A., Merlini, L., Boriani, G., Gallina, M., Morandi, L., Politano, L. *et al.* (2003) Mutation analysis of the lamin A/C gene (LMNA) among patients with different cardiomyopathy phenotypes. *J. Med. Genet.*, **40**, e132.
29. Arbustini, E., Pilotto, A., Repetto, M., Grasso, M., Negri, A., Diegoli, M., Campana, C., Scelsi, L., Baldini, E., Gavazzi, A. *et al.* (2002) Autosomal dominant dilated cardiomyopathy with atrioventricular block: a lamin A/C defect-related disease. *J. Am. Coll. Cardiol.*, **39**, 981–990.
30. van der Kooij, A.J., Ledderhof, T.M., de Voogt, W.G., Res, C.J., Bouwsma, G., Troost, D., Busch, H.F., Becker, A.E. and de Visser, M. (1996) A newly recognized autosomal dominant limb girdle muscular dystrophy with cardiac involvement. *Ann. Neurol.*, **39**, 636–642.
31. Karkkainen, S., Helio, T., Miettinen, R., Tuomainen, P., Peltola, P., Rummukainen, J., Ylitalo, K., Kaartinen, M., Kuusisto, J., Toivonen, L. *et al.* (2004) A novel mutation, Ser143Pro, in the lamin A/C gene is common in Finnish patients with familial dilated cardiomyopathy. *Eur. Heart J.*, **25**, 1–9.
32. Sebillon, P., Bouchier, C., Bidot, L.D., Bonne, G., Ahamed, K., Charron, P., Drouin-Garraud, V., Millaire, A., Desrumeaux, G., Benaiche, A. *et al.* (2003) Expanding the phenotype of LMNA mutations in dilated cardiomyopathy and functional consequences of these mutations. *J. Med. Genet.*, **40**, 560–567.
33. Mercuri, E., Poppe, M., Quinlivan, R., Messina, S., Kinali, M., Demay, L., Bourke, J., Richard, P., Sewry, C., Pike, M. *et al.* (2004) Extreme variability of phenotype in patients with an identical missense mutation in the lamin a/c gene: from congenital onset with severe phenotype to milder classic Emery–Dreifuss variant. *Arch. Neurol.*, **61**, 690–694.
34. Ben Yaou, R., Demay, L., Richard, P., Eymard, B., Urtizberea, J.A., Duboc, D., Muntoni, F., Wehnert, M., Toniolo, D., Merlini, L. *et al.* (2002) Clinical analysis of 32 patients carrying R453W LMNA mutation. *Neuromusc. Disord.*, **12**, 721.
35. Oliver, P.M., Fox, J.E., Kim, R., Rockman, H.A., Kim, H.S., Reddick, R.L., Pandey, K.N., Milgram, S.L., Smithies, O. and Maeda, N. (1997) Hypertension, cardiac hypertrophy, and sudden death in mice lacking natriuretic peptide receptor A. *Proc. Natl Acad. Sci. USA*, **94**, 14730–14735.
36. Djouadi, F., Weinheimer, C.J., Saffitz, J.E., Pitchford, C., Bastin, J., Gonzalez, F.J. and Kelly, D.P. (1998) A gender-related defect in lipid metabolism and glucose homeostasis in peroxisome proliferator-activated receptor alpha-deficient mice. *J. Clin. Invest.*, **102**, 1083–1091.
37. Kadokami, T., McTiernan, C.F., Kubota, T., Frye, C.S. and Feldman, A.M. (2000) Sex-related survival differences in murine cardiomyopathy are associated with differences in TNF-receptor expression. *J. Clin. Invest.*, **106**, 589–597.
38. Olsson, M.C., Palmer, B.M., Leinwand, L.A. and Moore, R.L. (2001) Gender and aging in a transgenic mouse model of hypertrophic cardiomyopathy. *Am. J. Physiol. Heart Circ. Physiol.*, **280**, H1136–H1144.
39. Haghighi, K., Schmidt, A.G., Hoit, B.D., Brittsan, A.G., Yatani, A., Lester, J.W., Zhai, J., Kimura, Y., Dorn, G.W., II, MacLennan, D.H. *et al.* (2001) Superinhibition of sarcoplasmic reticulum function by phospholamban induces cardiac contractile failure. *J. Biol. Chem.*, **276**, 24145–24152.
40. Freshour, J.R., Chase, S.E. and Vikstrom, K.L. (2002) Gender differences in cardiac ACE expression are normalized in androgen-deprived male mice. *Am. J. Physiol. Heart Circ. Physiol.*, **283**, H1997–H2003.
41. Xin, H.B., Senbonmatsu, T., Cheng, D.S., Wang, Y.X., Copello, J.A., Ji, G.J., Collier, M.L., Deng, K.Y., Jeyakumar, L.H., Magnuson, M.A. *et al.* (2002) Oestrogen protects FKBP12.6 null mice from cardiac hypertrophy. *Nature*, **416**, 334–338.
42. Dalloz, F., Osinska, H. and Robbins, J. (2001) Manipulating the contractile apparatus: genetically defined animal models of cardiovascular disease. *J. Mol. Cell. Cardiol.*, **33**, 9–25.
43. di Barletta, M.R., Ricci, E., Galluzzi, G., Tonali, P., Mora, M., Morandi, L., Romorini, A., Voit, T., Orstavik, K.H., Merlini, L. *et al.* (2000) Different mutations in the LMNA gene cause autosomal dominant and autosomal recessive Emery–Dreifuss muscular dystrophy. *Am. J. Hum. Genet.*, **66**, 1407–1412.
44. Burke, B. and Stewart, C.L. (2002) Life at the edge: the nuclear envelope and human disease. *Nat. Rev. Mol. Cell. Biol.*, **3**, 575–585.
45. Lammerding, J., Schulze, P.C., Takahashi, T., Kozlov, S., Sullivan, T., Kamm, R.D., Stewart, C.L. and Lee, R.T. (2004) Lamin A/C deficiency causes defective nuclear mechanics and mechanotransduction. *J. Clin. Invest.*, **113**, 370–378.
46. Kress, C., Vandormael-Pourmin, S., Baldacci, P., Cohen-Tannoudji, M. and Babinet, C. (1998) Nonpermissiveness for mouse embryonic stem (ES) cell derivation circumvented by a single backcross to 129/Sv strain: establishment of ES cell lines bearing the Omd conditional lethal mutation. *Mamm. Genome*, **9**, 998–1001.
47. Bunting, M., Bernstein, K.E., Greer, J.M., Capecchi, M.R. and Thomas, K.R. (1999) Targeting genes for self-excision in the germ line. *Genes Dev.*, **13**, 1524–1528.
48. Tanaka, N., Dalton, N., Mao, L., Rockman, H.A., Peterson, K.L., Gottshall, K.R., Hunter, J.J., Chien, K.R. and Ross, J., Jr (1996) Transthoracic echocardiography in models of cardiac disease in the mouse. *Circulation*, **94**, 1109–1117.
49. Le Menuet, D., Isnard, R., Bichara, M., Viengchareun, S., Muffat-Joly, M., Walker, F., Zennaro, M.C. and Lombes, M. (2001) Alteration of cardiac and renal functions in transgenic mice overexpressing human mineralocorticoid receptor. *J. Biol. Chem.*, **276**, 38911–38920.
50. Meneton, P., Bloch-Faure, M., Hagege, A.A., Ruetten, H., Huang, W., Bergaya, S., Ceiler, D., Gehring, D., Martins, I., Salmon, G. *et al.* (2001) Cardiovascular abnormalities with normal blood pressure in tissue kallikrein-deficient mice. *Proc. Natl Acad. Sci. USA*, **98**, 2634–2639.
51. Moll, J., Barzaghi, P., Lin, S., Bezakova, G., Lochmuller, H., Engvall, E., Muller, U. and Ruegg, M.A. (2001) An agrin minigene rescues dystrophic symptoms in a mouse model for congenital muscular dystrophy. *Nature*, **413**, 302–307.
52. Dubowitz, V. (1985) A practical approach. In Dubowitz, V. (ed.) *Muscle Biopsy*. Bailliere Tindale, London, pp. 19–40.
53. Toussaint, M., Planche, C., Duboc, D., Pfister, A., Da Lage, C. and Guerin, F. (1987) Left ventricular ultrastructure in pulmonary stenosis and in tetralogy of Fallot. *Virchows Arch. A Pathol. Anat. Histopathol.*, **411**, 33–38.
54. Picard, F., Gehin, M., Annicotte, J., Rocchi, S., Champy, M.F., O'Malley, B.W., Chambon, P. and Auwerx, J. (2002) SRC-1 and TIF2 control energy balance between white and brown adipose tissues. *Cell*, **111**, 931–941.
55. Rocchi, S., Picard, F., Vamecq, J., Gelman, L., Potier, N., Zeyer, D., Dubuquoy, L., Bac, P., Champy, M.F., Plunket, K.D. *et al.* (2001) A unique PPARgamma ligand with potent insulin-sensitizing yet weak adipogenic activity. *Mol. Cell*, **8**, 737–747.
56. Sewry, C.A., Brown, S.C., Mercuri, E., Bonne, G., Feng, L., Camici, G.E., Morris, G.E. and Muntoni, F. (2001) Skeletal muscle pathology in autosomal dominant Emery–Dreifuss muscular dystrophy with lamin A/C mutations. *Neuropathol. Appl. Neurobiol.*, **27**, 281–290.
57. Kitaguchi, T., Matsubara, S., Sato, M., Miyamoto, K., Hirai, S., Schwartz, K. and Bonne, G. (2001) A missense mutation in the exon 8 of lamin A/C gene in a Japanese case of autosomal dominant limb-girdle muscular dystrophy and cardiac conduction block. *Neuromusc. Disord.*, **11**, 542–546.
58. Fidzianska, A. and Hausmanowa-Petrusewicz, I. (2003) Architectural abnormalities in muscle nuclei. Ultrastructural differences between X-linked and autosomal dominant forms of EDMD. *J. Neurol. Sci.*, **210**, 47–51.
59. Emery, A.E.H. (2000) Emery–Dreifuss muscular dystrophy—a 40 year retrospective. *Neuromusc. Disord.*, **10**, 228–232.